



**HAL**  
open science

## **B0 field distortions monitoring and correction for 3D non-Cartesian fMRI acquisitions using a field camera: Application to 3D-SPARKLING at 7T**

Zaineb Amor, Chaithya Giliyar Radhakrishna, Caroline Le Ster, Guillaume Daval-Fr erot, Nicolas Boulant, Franck Mauconduit, Christian Mirkes, Philippe Ciuciu, Alexandre Vignaud

### ► **To cite this version:**

Zaineb Amor, Chaithya Giliyar Radhakrishna, Caroline Le Ster, Guillaume Daval-Fr erot, Nicolas Boulant, et al.. B0 field distortions monitoring and correction for 3D non-Cartesian fMRI acquisitions using a field camera: Application to 3D-SPARKLING at 7T. Joint Annual Meeting ISMRM-ESMRMB & ISMRT 31st Annual Meeting, May 2022, London, United Kingdom. hal-03901242

**HAL Id: hal-03901242**

**<https://hal.science/hal-03901242>**

Submitted on 15 Dec 2022

**HAL** is a multi-disciplinary open access archive for the deposit and dissemination of scientific research documents, whether they are published or not. The documents may come from teaching and research institutions in France or abroad, or from public or private research centers.

L'archive ouverte pluridisciplinaire **HAL**, est destin ee au d ep ot et  a la diffusion de documents scientifiques de niveau recherche, publi es ou non,  emanant des  tablissements d'enseignement et de recherche franais ou  trangers, des laboratoires publics ou priv es.

# $B_0$ field distortions monitoring and correction for 3D non-Cartesian fMRI acquisitions using a field camera: Application to 3D-SPARKLING at 7T

Zaineb Amor<sup>1</sup>, Chaithya G.R.<sup>1,2</sup>, Caroline Le Ster<sup>1</sup>, Guillaume Daval-Fr erot<sup>1,2,3</sup>, Nicolas Boulant<sup>1</sup>, Franck Mauconduit<sup>1</sup>, Christian Mirkes<sup>4</sup>, Philippe Ciuciu<sup>1,2</sup>, and Alexandre Vignaud<sup>1</sup>

<sup>1</sup>Universit  Paris-Saclay, CEA, Neurospin, CNRS, Gif-sur-Yvette, France, <sup>2</sup>Universit  Paris-Saclay, Inria, Parietal, Palaiseau, France, <sup>3</sup>Siemens Healthcare SAS, Saint Denis, France, <sup>4</sup>Skope Magnetic Resonance Technologies AG, Zurich, Switzerland

## Synopsis

The benefit of retrospective correction of static and dynamic  $B_0$  field imperfections was studied on non-Cartesian compressed sensing-based acquisition patterns by taking as an example 3D-SPARKLING encoding scheme. Long-TR dynamic acquisitions of T2\*-weighted MRI (fMRI-like) volumes were acquired at 7T, retrospectively corrected, and the evaluation of the corrections was based on the image quality and the gain in temporal signal-to-noise ratio (tSNR). We found that correcting for the static and dynamic 0<sup>th</sup> order contributions is enough to enhance the image quality and tSNR significantly (up to 22% gain in median tSNR).

## Introduction

In fMRI, understanding the different sources of confounds and correcting them is an important concern<sup>1-3</sup>. Magnetic field fluctuations alter the Larmor frequency, hence the nuclear spins phase which encodes the spatial information in MRI. Dynamic field perturbations cause changes in the recorded NMR signal that are unrelated to neuro-vascular coupling and as such can be considered as confounds. Static but spatially varying field distortions are not an issue for the data temporal stability, yet induce signal loss in tissue-air interfaces, especially in non-Cartesian settings and at higher magnetic fields (3T and higher). To address this issue, one can account for static and dynamic  $B_0$  perturbations retrospectively in the signal model during image reconstruction<sup>4</sup>. More specifically, additional measurements can be acquired and used in the extended signal model. The static contribution is usually measured with a  $B_0$  map. The dynamic fluctuations can be monitored using navigators but a new method that uses NMR probes<sup>5</sup> to monitor the field dynamics concurrently to the imaging process<sup>6</sup> was explored in literature for anatomical and functional MRI<sup>7-10</sup>. Hereafter, we use this NMR probes system, namely the Skope Clip-on Camera, to measure field fluctuations and the actual k-space trajectories to assess the potential benefit of correcting  $B_0$  perturbations on 3D-SPARKLING<sup>11-13</sup> fMRI-like data at 7T (Fig.1-a).

## Theory

In a 3D framework, the extended received signal  $S(t)$  model can be written according to the equation below where  $x(\mathbf{r})$  is the density source at the 3D spatial position  $\mathbf{r}$  and  $\mathbf{k}(t)$  is the 3D k-space position at time  $t$ .  $\Delta B_{0,stat}(\mathbf{r})$  reflects the static off-resonance at  $\mathbf{r}$ .  $\Delta B_{0,dyn}$  reflects the global, slowly varying 0<sup>th</sup> order contribution of the dynamic field fluctuations and is considered constant during a shot.  $\delta\mathbf{k}(t)$  is the dynamic first-order deviation from the nominal position defined by  $\mathbf{k}(t)$ . Given measurements of  $\Delta B_{0,stat}(\mathbf{r})$ ,  $\Delta B_{0,dyn}$  and  $\delta\mathbf{k}(t)$ , we can include them in the reconstruction algorithm and have a model that better reflects the actual acquisition process. In a parallel imaging framework, this model is considered for all shots and channels.

$$S(t) = \exp(2i\pi\Delta B_{0,dyn} \times t) \int_{\mathbf{r}} x(\mathbf{r}) \exp(2i\pi\Delta B_{0,stat}(\mathbf{r}) \times t) \exp(-2i\pi(\mathbf{k}(t) + \delta\mathbf{k}(t)) \circ \mathbf{r}) d\mathbf{r}$$

## Methods

Acquisition strategy: Functional-like data was collected on a single healthy volunteer at 7T (Siemens Magnetom) using a 1Tx-32Rx Nova head coil with 3D-SPARKLING for the acquisition parameters reported in Fig.1-b. Due to constraints related to the field monitoring system (Skope's Clip-on Camera), the shortest unitary TR we could choose was 150ms. This impacted the volumetric TR. A gradient recalled echo 2D (GRE 2D) sequence with two echoes (Fig.1-b) was used to estimate the  $B_0$  map. External sensitivity maps were acquired using a gradient recalled echo (GRE) sequence (Fig.1-b).

Common reconstruction strategy: 3D-SPARKLING volumes were reconstructed independently from each other using a nonlinear multi-coil compressed sensing reconstruction that promotes sparsity in the wavelet domain<sup>14</sup>. The reconstruction was calibrated using the external sensitivity maps. Implementation and details can be found in<sup>15-16</sup>.

Additional corrections: To correct for the dynamic fluctuations at the 0<sup>th</sup> order, the raw NMR data needs to be demodulated by  $-2i\pi\Delta B_{0,dyn} \times t$  prior to the reconstruction. The field camera, allows us to measure  $k_0(t) = 2i\pi\Delta B_{0,dyn} \times t$  at each time point  $t$ , thus, we used those measurements for the demodulation. To account for the first-order dynamic field fluctuations, the non-uniform Fourier operator was defined over the measured k-space trajectories (Fig.2). Unlike the Skope system, the scanner applies an Eddy currents compensation phase (ECCPhase) on the recorded signal upon reception. This means that  $\Delta B_{0,dyn}$  or  $k_0(t)$  accounts for Eddy currents-induced fluctuations whereas they are already corrected by the scanner. To be consistent, we retrospectively decompensated the correction applied by the scanner using a simulation of the ECCPhase. Finally, static  $\Delta B_0$  was corrected by including the acquired  $B_0$  map in the definition of the extended Fourier operator (see "Theory"), implementing the method proposed in<sup>17</sup>. Fig.2 summarizes the data processing pipeline and details the different combinations of corrections that were applied.

Evaluation: The comparisons were based on the impact on image quality (assessed visually) and on the tSNR (an objective and relevant criterion for fMRI).

## Results and Discussion

Fig.3-a shows the effect of the different corrections on image quality: The main difference comes from  $\Delta B_{0,stat}$  correction. Fig.3-b shows that  $\Delta B_{0,dyn}$  smoothes the mean difference image slightly. Fig.4 and Fig.5-a show, that in terms of tSNR, the highest benefit is achieved when correcting for both dynamic and static contributions (up to 26% gain in median tSNR for the best scenario). Additionally, the gain brought by  $\delta\mathbf{k}(t)$  is modest when compared to  $\Delta B_{0,stat}$  and  $\Delta B_{0,dyn}$ . However, Fig.5-b shows that an increase in the median tSNR comes with an increase in the standard deviation as well: this needs to be considered carefully. A Mood test between the corrected and uncorrected data proved that the gain in median tSNR is statistically significant.

## Conclusion

Correcting for  $\Delta B_{0,stat}$  enhances image quality greatly, pairing it with  $\Delta B_{0,dyn}$  correction significantly boosts the tSNR. The gain in tSNR when including  $\delta \mathbf{k}(t)$  in the reconstruction is lesser. We also highlight the limitations :

- 1) The external  $B_0$  map constitutes a limitation since patient movement will cause misalignment with the fMRI scans and consequently impact the correction.
  - 2) The current volumetric TR used is too long for a real fMRI application.
- This proof of concept will be extended for a better temporal resolution.

## Acknowledgements

Leducq Foundation (Large Equipment ERPT program, NEUROVASC7T project) provided financial support for this work. Chaithya G.R. was supported by the CEA NUMERICS program, which has received funding from the European Union's Horizon 2020 research and innovation program under the Marie Skłodowska-Curie grant agreement No 800945.

## References

- <sup>1</sup> K. Murphy et al. Resting-state fMRI Confounds and Cleanup. *Neuroimage*, 80:349–59, 2013.
- <sup>2</sup> M. G. Bright et al. Cleaning Up the fMRI Time Series: Mitigating Noise with Advanced Acquisition and Correction Strategies. *Neuroimage*, 154:1–3, 2017.
- <sup>3</sup> C. Caballero-Gaudes et al. Methods for Cleaning the Bold fMRI Signal. *Neuroimage*, 154:128–149, 2017.
- <sup>4</sup> Mariya Doneva. Mathematical Models for Magnetic Resonance Imaging Reconstruction. *IEEE Signal Processing Magazine*, 37(1):24–32, 2020.
- <sup>5</sup> N. De Zanche et al. NMR Probes for Measuring Magnetic Fields and Field Dynamics in MR Systems. *Magnetic Resonance in Medicine*, 60(1):176–86, 2008.
- <sup>6</sup> C. Barmet et al. Spatiotemporal Magnetic Field Monitoring for MR. *Magnetic Resonance in Medicine*, 60(1):187–197, 2008.
- <sup>7</sup> L. Kasper et al. Monitoring, Analysis, and Correction of Magnetic Field Fluctuations in Echo Planar Imaging Time Serie. *Magnetic Resonance in Medicine*, 74(2):396–409, 2015.
- <sup>8</sup> S.J. Vannesjo et al. Retrospective Correction of Physiological Field Fluctuations in High-field Brain MRI Using Concurrent Field Monitoring. *Magnetic Resonance in Medicine*, 73(5):1833–1843, 2015.
- <sup>9</sup> J. M. Schwarz et al. Correction of Physiological Field Fluctuations in High- and Low-resolution 3D-EPI Acquisitions at 7 Tesla. *ISMRM*, 2019.
- <sup>10</sup> S. Bollmann et al. Analysis and Correction of Field Fluctuations in fMRI Data Using Field Monitoring. *Neuroimage*, 154:92–105, 2017.
- <sup>11</sup> C. Lazarus et al. SPARKLING: Variable-density k-space Filling Curves for Accelerated T2\*-weighted MRI. *Magnetic Resonance in Medicine*, 81(6):3643–3661, 2019.
- <sup>12</sup> C. Lazarus et al. 3D Variable-density SPARKLING Trajectories for High-resolution T2\*-weighted Magnetic Resonance Imaging. *NMR in Biomedicine*, 33(9), 2020.
- <sup>13</sup> G.R. Chaithya et al. Optimizing Full 3D SPARKLING Trajectories for High Resolution T2\*-weighted Magnetic Resonance Imaging. under review at *IEEE Transactions on Medical Imaging*, 2021.
- <sup>14</sup> L. El Gueddari et al. Self-calibrating Nonlinear Reconstruction Algorithms for Variable Density Sampling and Parallel Reception MRI. *IEEE 10th Sensor Array and Multichannel Signal Processing Workshop (SAM)*, 2018.
- <sup>15</sup> [https://github.com/CEA\\_COSMIC/pysap-mri](https://github.com/CEA_COSMIC/pysap-mri).
- <sup>16</sup> S. Farrens et al. Pysap: Python Sparse Data Analysis Package for Multidisciplinary Image Processing. *Astronomy and Computing*, 32, 2020.
- <sup>17</sup> J. A. Fessler et al. Toeplitz-based Iterative Image Reconstruction for MRI with Correction for Magnetic Field Inhomogeneity. *IEEE Transactions On Signal Processing*, 53(9):3393–3402, 2005.
- <sup>18</sup> L. El Gueddari et al. Calibrationless Oscar-based Image Reconstruction in Compressed Sensing Parallel MRI. *IEEE 16th International Symposium on Biomedical Imaging*, 2019.

## Figures

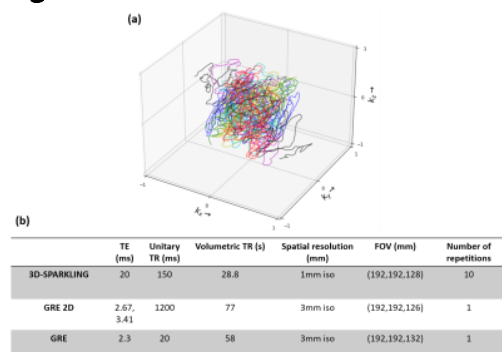


Fig.1: (a) Seven color-coded shots from 3D-SPARKLING readouts. 3D-SPARKLING is a projected gradient descent algorithm that generates multi-shot patterns in agreement with compressed sensing theories that follow a prescribed target density. The projection step ensures that the shots meet the hardware constraints. Paired with nonlinear reconstruction methods<sup>14,18</sup>, 3D-SPARKLING patterns allow for higher acceleration factors and therefore reduced acquisition times. (b) Details of the different sequences used in the experimental protocol.

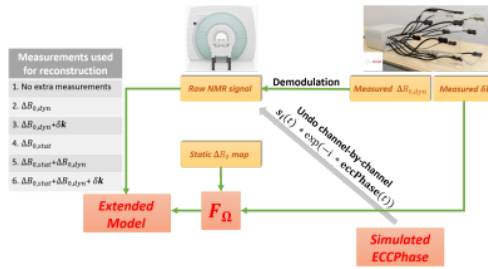


Fig.2: An explanatory scheme of the different steps of the corrections and the different measurements combinations used in the extended signal model.  $F_{\Omega}$  is the extended Fourier transform defined over the pattern  $\Omega$  defined along the measured trajectories and that takes into account the prior  $B_0$  map.

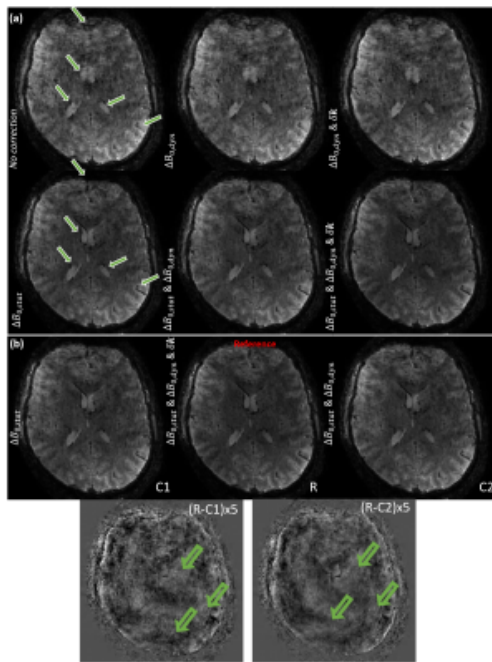


Fig.3: (a) The mean image computed from the time-series for each correction setup. The arrows show how  $\Delta B_{0,stat}$  induced artifacts are reduced. (b) The mean image computed from the time-series reconstructed with the three setups involving  $\Delta B_{0,stat}$  correction and the amplified difference images computed as indicated in the figure. The arrows show the effect of  $\Delta B_{0,dyn}$  on the mean difference image quality.

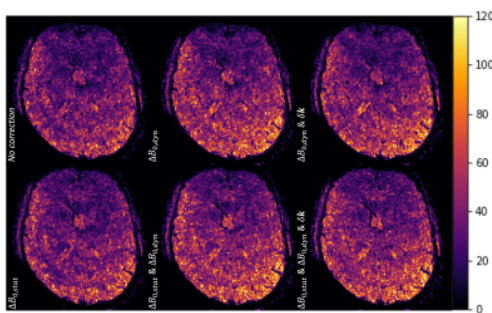


Fig.4: Temporal SNR maps for the different corrections: Observe how including the dynamic contributions improves the gain in tSNR along the edges of the brain, this means that motion-related fluctuations are corrected. Correcting for the static contribution, on the other hand, improves the point spread function (a better resolved image) and reduces signal loss in critical regions with air-tissue interfaces.

(a) Gain in % of native (no correction) median tSNR computed over the 3D masked brain induced by the different corrections

Type of correction applied	Gain in % of native (no correction) median tSNR computed over the 3D masked brain
$\Delta B_{0, dyn}$	12.69%
$\Delta B_{0, dyn} + \delta k$	14.51%
$\Delta B_{0, stat}$	6.693%
$\Delta B_{0, stat} + \Delta B_{0, dyn}$	22.693%
$\Delta B_{0, stat} + \Delta B_{0, dyn} + \delta k$	26.453%

(b) Boxplot of the relative change in % of native (no correction) tSNR on the 3D masked brain induced by the different corrections

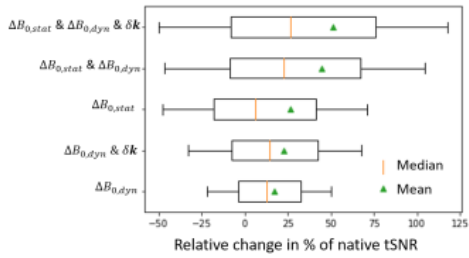


Fig.5: (a) A table summarizing the gain in median tSNR (in %) for the different correction setups. (b) Boxplot of the relative change in tSNR in % compared to the native (no correction) tSNR computed over the 3D masked brain. A Mood test proved that the native (no correction) median tSNR is significantly improved (at a statistical level of significance of  $10^{-3}$ ) with the five different corrections implemented.